CLIMATOLOGY

# Prolonged drying trend coincident with the demise of Norse settlement in southern Greenland

**Boyang Zhao[1]*†, Isla S. Castañeda[1]*, Jeffrey M. Salacup[1], Elizabeth K. Thomas[2], William C. Daniels[1], Tobias Schneider[1]‡, Gregory A. de Wet[1,3], Raymond S. Bradley[1]***



**Declining temperature has been thought to explain the abandonment of Norse settlements, southern Greenland, in the early 15th century, although limited paleoclimate evidence is available from the inner settlement region itself. Here, we reconstruct the temperature and hydroclimate history from lake sediments at a site adjacent to a former Norse farm. We find no substantial temperature changes during the settlement period but rather that the region experienced a persistent drying trend, which peaked in the 16th century. Drier climate would have notably reduced grass production, which was essential for livestock overwintering, and this drying trend is concurrent with a Norse diet shift. We conclude that increasingly dry conditions played a more important role in undermining the viability of the Eastern Settlement than minor temperature changes.**

## INTRODUCTION

Norse settlers developed the Eastern Settlement on southern Greenland in 985 CE, and other settlers subsequently expanded the settlements on the shores of the fjords to the south and southwest of Narsarsuaq (fig. S1) (*1*, *2*). The inhabitants relied primarily on raising livestock on cleared pastureland for sustenance (*3*), and the estimated population reached about 2000 people (*4*). Despite the success of the settlements, the region was largely abandoned by the early 15th century (*1*, *2*). As some previous investigations note, this abandonment could have resulted from multiple issues, including climate change, management failure, economic collapse, or social stratification (*1*, *5*, *6*). Nevertheless, climate change has long been considered an important contributing factor (*1*). Southern Greenland was always near the limit of agriculture for the Norse settlers, although they had experience in stock-raising and farming in similarly challenging environments in Iceland and Norway (*2*, *7*). For example, in wintertime, cattle and some sheep and goats had to be kept in the warm dark byres, and by spring, many cattle were too weak to move and the Norse farmers had to carry them out to pasture (*2*). Therefore, it is likely that a changing climate would have imposed considerable stress on the entire Eastern Settlement community (*7*).

Temperature change has often been cited as an explanation for the demise of the Eastern Settlement, on the basis of the notion that the Norse arrived during a relatively warm interval and were able to survive until temperatures declined during the Little Ice Age (*1*). However, most paleotemperature reconstructions from southern Greenland do not have sufficient temporal resolution to capture such a transition, are not directly calibrated to temperature, or are located relatively far from the inner settlement region (*8*–*13*). Furthermore, modern Greenlandic agricultural production is sensitive to rainfall variability (*14*, *15*), but there is currently little information on hydroclimate during the Norse Period. To address this matter, we report records of past temperature and hydroclimate at a multidecadal (~30-year) resolution, using branched glycerol dialkyl glycerol tetraethers (brGDGTs) and leaf wax hydrogen isotopes ($\delta^2H$) in lake sediments, from Lake 578, which is adjacent to a former Norse farm and is only ~9 km from Qassiarsuk (Brattahlíð), where the Norse had some of the largest farms in the Eastern Settlement (fig. S1) (*2*). On the basis of our temperature and hydroclimate reconstructions, we show that there was no abrupt temperature decline around the time when the Norse settlements were abandoned but that summers became increasingly dry throughout the entire Norse occupancy period.

## RESULTS AND DISCUSSION

### Southern Greenland temperature variability during the Late Holocene

brGDGTs, membrane lipids produced by bacteria (*16*, *17*), are used to reconstruct temperature (Supplementary Materials). With a 3-year sediment trap experiment in Lake 578, situated in the Eastern Settlement with Norse ruins within the catchment (Supplementary Materials), the $MBT'_{5ME}$ index (methylation of branched tetraethers) (*18*) is shown to be significantly correlated with summer water temperature (*19*). This allows us to apply $MBT'_{5ME}$ to a well-dated sediment core (fig. S5) to reconstruct summer water temperature extending back to ~375 CE (Supplementary Materials). Our summer temperature reconstruction shows an overall gradual cooling trend (−0.07°C/100 years) over the entire time span, tracking changes in summer insolation (Fig. 1). Superimposed on the overall cooling trend are several short-lived subcentury scale oscillations.

The Lake 578 temperature reconstruction shows a general agreement with other local records and with a pan-Arctic summer temperature reconstruction (*20*), indicating a prominent cooling trend and coinciding with decreasing summer insolation at 61°N (Fig. 1, A to C) (*21*). The Lake 578 record also tracks southern Greenland ice sheet fluctuations, which advanced around 1450 to 1750 CE (*22*) (Fig. 1D). One outlet glacier, the Kiagtût Sermiat, reached its late Holocene maximum between approximately 440 and 610 CE (*23*). However, this is considered as an exception and is unlike the general pattern of other ice margins in southern Greenland. It is possible that the

[1]Department of Geosciences, University of Massachusetts Amherst, Amherst, MA 01003, USA. [2]Department of Geology, University at Buffalo, Buffalo, NY 14260, USA. [3]Department of Geosciences, Smith College, Northampton, MA 01063, USA.
*Corresponding author. Email: boyangzhao@geo.umass.edu (B.Z.); isla@geo.umass.edu (I.S.C.); rbradley@geo.umass.edu (R.S.B.)
†Present Address: Department of Earth, Environmental, and Planetary Sciences, Brown University, Providence, RI 02912, USA.
‡Present Address: Lamont-Doherty Earth Observatory of Columbia University, Palisades, NY 10964, USA.

Kiagtût Sermiat was influenced by local topographic conditions or internal dynamics and is not representative of regional glacier fluctuations in southern Greenland (*22*).

Unlike the long-term cooling trend shown in our study and from Lake Igaliku in the inner fjords (Fig. 1E) (*8*), two records from the outer coastal region show a general warming trend during the Late Holocene (Fig. 1, F and G) (*10*, *11*). This is likely due to the coastal influence of the Eastern Greenland Current (EGC) and Irminger Current (IC). The EGC is a cold, low-salinity current that exports sea ice from the Arctic along the eastern coast of Greenland. The IC is a branch of the North Atlantic Current that brings relatively warm water southwestward toward southern Greenland. The two currents mix around Cape Farewell and then move northwestward along the coast of western Greenland, where the sea ice quickly melts (*10*). Diatom-based August sea surface temperatures (SSTs) from marine sediment cores (fig. S1) suggest warming of both the EGC and IC in the past ~2000 years (Fig. 1, H and I) (*24*, *25*), which is thought to have caused the warming along the outer coast of southern Greenland (*10*, *11*). However, at more inland parts of the Eastern Settlement, the climate is more continental, the influence of the ocean is reduced, and summer insolation played a more important role, as seen in other Holocene records from Greenland (*26*, *27*).

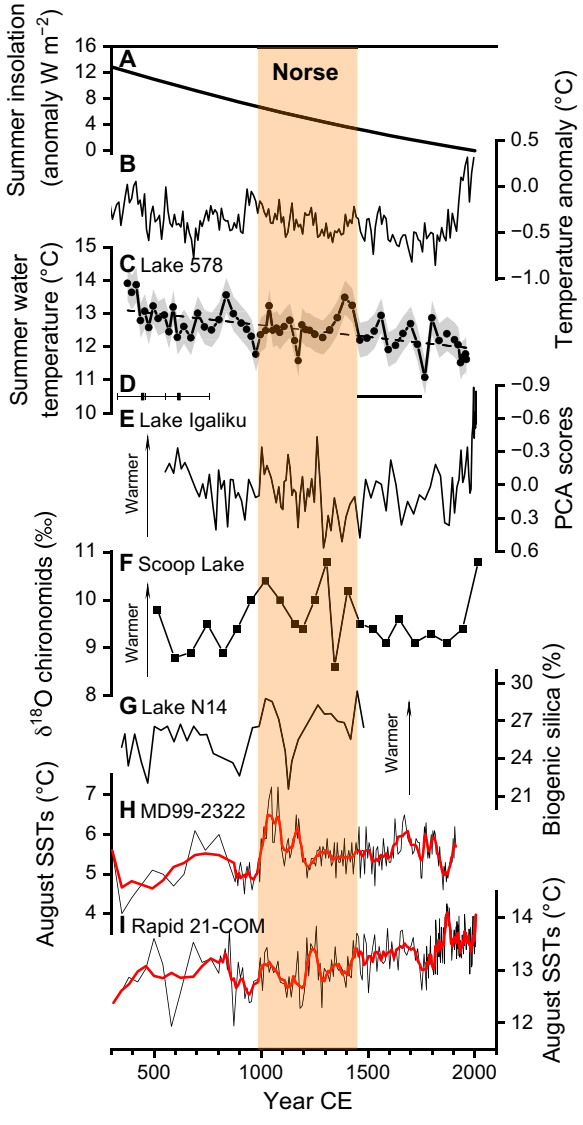


**Fig. 1. Temperature profiles from southern Greenland and the related driving factors.** (**A**) Summer insolation anomaly at 61° N (*21*). (**B**) Arctic summer temperature anomaly based on a synthesis of multiple Arctic records (*20*). (**C**) Our brGDGT-inferred summer water temperature from Lake 578. Gray shading represents the calibration errors of ±0.52°C (*19*). The dashed line represents the linear trend. Note that the temperature reconstruction is truncated at 7 cm because of the unconstrained "core-top cooling" for the sedimentary MBT'$_{5ME}$ index (Supplementary Materials). (**D**) Southern Greenland region glacier extent. The solid squares are $^{10}$Be-dated moraine age near Narsarsuaq (*23*), and the thick line indicates the readvanced period of the south Greenland ice margin (*22*). (**E**) Principal component analysis (PCA) scores of the Lake Igaliku chironomid samples (*8*). (**F**) $\delta^{18}$O values of Scoop Lake chironomids (*11*). (**G**) Biogenic silica from Lake N14 (*10*). (**H**) Diatom-based August SSTs from core MD99-2322 from the SE Greenland shelf (*24*). (**I**) Reconstructed August SSTs from core Rapid 21-COM, the Reykjanes Ridge (*25*). Orange bar indicates the time span of Norse settlement. The red lines are 5-point running mean. See fig. S1 for site locations.

It is worth noting that August SSTs of the EGC were anomalously warm during the Medieval period (*24*), and similar warmth is also seen in the two outer fjord records (*10*, *11*). However, Lake 578 in the inner settlement region shows only moderate warmth at this time, so the Norse settlements did not experience a particularly warm Medieval period. Although there is evidence for a long-term cooling trend in our record, temperature did not decline during the period of the Norse settlement, and there is no evidence of unusually low temperatures around the time when the Eastern Settlement was abandoned (fig. S7). The late 14th century was one of the warmest periods of the entire record.

## Southern Greenland hydroclimate reconstruction and the linkage to the North Atlantic Oscillation

To estimate changes in hydroclimate, we measured the deuterium isotopic composition ($\delta^2$H) of both long- ($n$C$_{29}$) and mid-chain ($n$C$_{23}$) $n$-alkanes (Fig. 2A), which are sourced predominantly from terrestrial higher plants and aquatic plants, respectively (*28*, *29*). Plant wax $\delta^2$H reflects the hydrogen isotope composition of the source water the plant uses to make its leaf waxes with an offset due to biosynthetic fractionation (*30*). Here, we specifically target aquatic and terrestrial wax isotopes that are influenced by the same processes, but the evaporative enrichment of terrestrial plant leaf water allows us to investigate summer relative humidity (ΔRH) with a dual-biomarker model (*31*, *32*). We note that although the sedimentary leaf wax source attributions are ambiguous in some west Greenland lakes (*33*), in Lake 578, multiple lines of evidence suggest that the mid- and long-chain $n$-alkanes in sediments are mainly sourced from submerged and terrestrial plants, respectively. For example, the dominant submerged plant, *Myriophyllum sibiricum*, has abundant C$_{23}$ $n$-alkanes. Detailed proxy interpretations are provided in the Supplementary Materials. Because they share the same ultimate water source, both the $\delta^2$H of C$_{23}$ and C$_{29}$ are generally in accordance with the oxygen isotopes of the DYE-3 ice core (Fig. 2B) (*34*).

Our reconstructed quantitative ΔRH from southern Greenland, normalized over 1950 to 2016 CE, indicates a persistent wet interval during 600 to 950 CE (Fig. 2C), before the arrival of the Norse. After ~950 CE, the Lake 578 record shows a long-term drying trend until the 16th century, becoming relatively stable thereafter. The hydroclimate variability is accompanied by changes in lake productivity (Fig. 2, E and F). Wetter periods are associated with higher concentrations of organic carbon and chlorins, and vice versa. On the basis

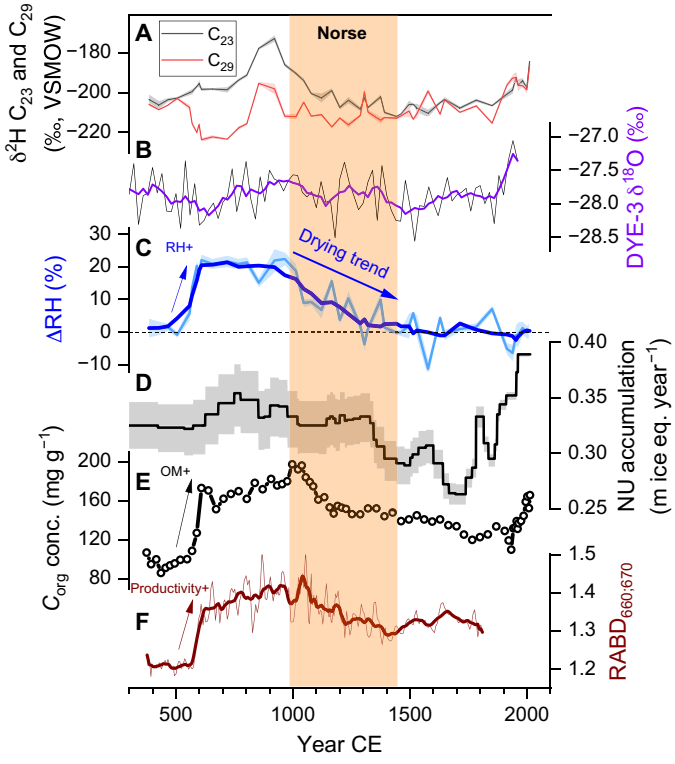


**Fig. 2. Hydroclimate profile from Lake 578, southern Greenland.** (**A**) Leaf wax $\delta^2$H of $C_{23}$ (aquatic) and $C_{29}$ (terrestrial) *n*-alkanes from Lake 578. The black and red shading represents 1 σ proxy uncertainty. (**B**) DYE-3 ice core oxygen isotopes (*34*). The thick violet line is the 5-point running mean. (**C**) ΔRH reconstruction from Lake 578 based on leaf wax $\delta^2$H and the dual-biomarker model (*31*). Blue shading represents the 90% confidence interval (CI), and the thick blue line is the 5-point running mean. (**D**) The optimum Nuussuaq (NU) ice cap accumulation history and the 10% least complex interval denoted with gray shades (*35*). (**E**) Concentrations of organic carbon from Lake 578 (Supplementary Materials). Higher values indicate a high organic matter (OM) content. (**F**) $RABD_{660;670}$ index (relative absorption band depth centered in 660 to 670 nm) from Lake 578, indicates the intensity of lake productivity (Supplementary Materials). The thick brown line is the 10-point running mean. Orange bar indicates the time span of Norse settlement. VSMOW, Vienna Standard Mean Ocean Water.

of observations from modern Arctic lakes, we speculate that this relationship arises from variations in nutrient transport from the catchment to the lake as moisture conditions vary. The drying trend we observe at Lake 578, from ~950 CE to the 16th century, is similar to hydroclimate shifts in west Greenland (Fig. 2D) (*35*). The average snow accumulation of the Nuussuaq ice cap decreased up to 20% during the transition from the Medieval period to the Little Ice Age (*35*). However, accumulation in west Greenland greatly increased since the early 18th century (*35*), while such a trend is not identified in the Lake 578 hydroclimate record. This suggests that the hydroclimatic conditions in west Greenland and southern Greenland have responded differently from anthropogenic warming. The North Atlantic Oscillation (NAO) is largely accountable for hydroclimate variability in southern Greenland (Fig. 3), but this influence does not extend to the location of the Nuussuaq ice cap. The NAO is defined in terms of air pressure differences between Iceland and the Azores, with a positive NAO index indicating anomalously high pressure over the Azores and vice versa (*36*). Although the NAO is most pronounced in the winter, it is a characteristic of all months of the year (*37*). In southern Greenland, precipitation amounts in June, July, and August are significantly correlated with the corresponding monthly NAO index (Fig. 3, A and B). The Greenland Blocking Index (GBI) describes the high-pressure blocking over Greenland and is broadly negatively correlated with the NAO (*38*). Under a positive GBI, the polar jet stream migrates northward, resulting in a negative precipitation anomaly in southern Greenland (*38*). In general, a negative summer NAO phase is associated with reduced precipitation in summer, with the opposite conditions in a positive summer NAO phase, contributing to a wet climate (Fig. 3, A and B). If the same teleconnection pattern prevailed in the past, this suggests that the wet interval (600 to 950 CE) was associated with a persistently positive NAO (*39*).

It is unclear whether a shift in the NAO caused the prolonged drying trend between ~950 CE and the early 16th century, since there is conflicting evidence based on different NAO reconstructions (*40*, *41*). The center of the NAO in the past may appear in different locations, making it challenging to assess the real NAO pattern with proxy-inferred NAO reconstructions (*42*). For example, some NAO reconstructions suggest persistent positive NAO mode during the Medieval period, while other studies contradict this notion (*40*, *41*). Moreover, a North Atlantic zonal wind profile reconstruction does not show a distinct trend in terms of the jet stream position and intensity in the past 1250 years (*43*). Nevertheless, our finding of increasingly arid conditions from southern Greenland throughout the Norse settlement period is robust and supported by multiple proxies.

## The impact of drought on the Norse farmers

Compared to the widely held theory that low temperatures led to the demise of the Eastern Settlements, our evidence shows a distinct hydroclimate shift during the Norse period, compared to only moderate temperature fluctuations (Fig. 4, A and B). Although the climate in southern Greenland is not conducive to animal husbandry, according to our reconstructions, the Norse farmers experienced climate conditions in the early years of Eastern Settlement that would have provided quite favorable growing conditions for agriculture in the region. Subsequently, increasingly dry conditions, as indicated by our ΔRH record, would have decreased the available pasturage in the growing season and thus limited fodder yields that were essential for the sustenance of animals during the winter (*44*). This challenge of limited water availability is illustrated by archeological evidence of irrigation channels in Igaliku (*44*, *45*). In addition, there was a gradual change in the diet of the Norse farmers over time, toward reliance on marine food sources (Fig. 4, C and D). The Norse diet relied primarily on terrestrial sources at the beginning of the settlement era and transitioned to marine-based food sources over time (*46*, *47*). The prolonged drying trend (Fig. 4B), perhaps exacerbated by warmer temperatures toward the end of the settlement period, is a plausible reason for a decline in the availability of meat from animals raised on Norse farms, forcing the farmers to hunt sea mammals, which was a more dangerous and uncertain activity (*2*). Meanwhile, the increased sea ice during the later settlement period may have hindered their marine harvesting and interfered with connections between the Norse community and Europe (*1*, *2*, *48*). Last, an inability to manage increasingly drier conditions would have hampered the resilience of the community, possibly leading to social instability and eventual abandonment.

Notably, the threat of droughts has been underscored for the local farmers from southern Greenland in the recent decades (*15*). In 2008, drought in southern Greenland caused a 50% reduction in yield

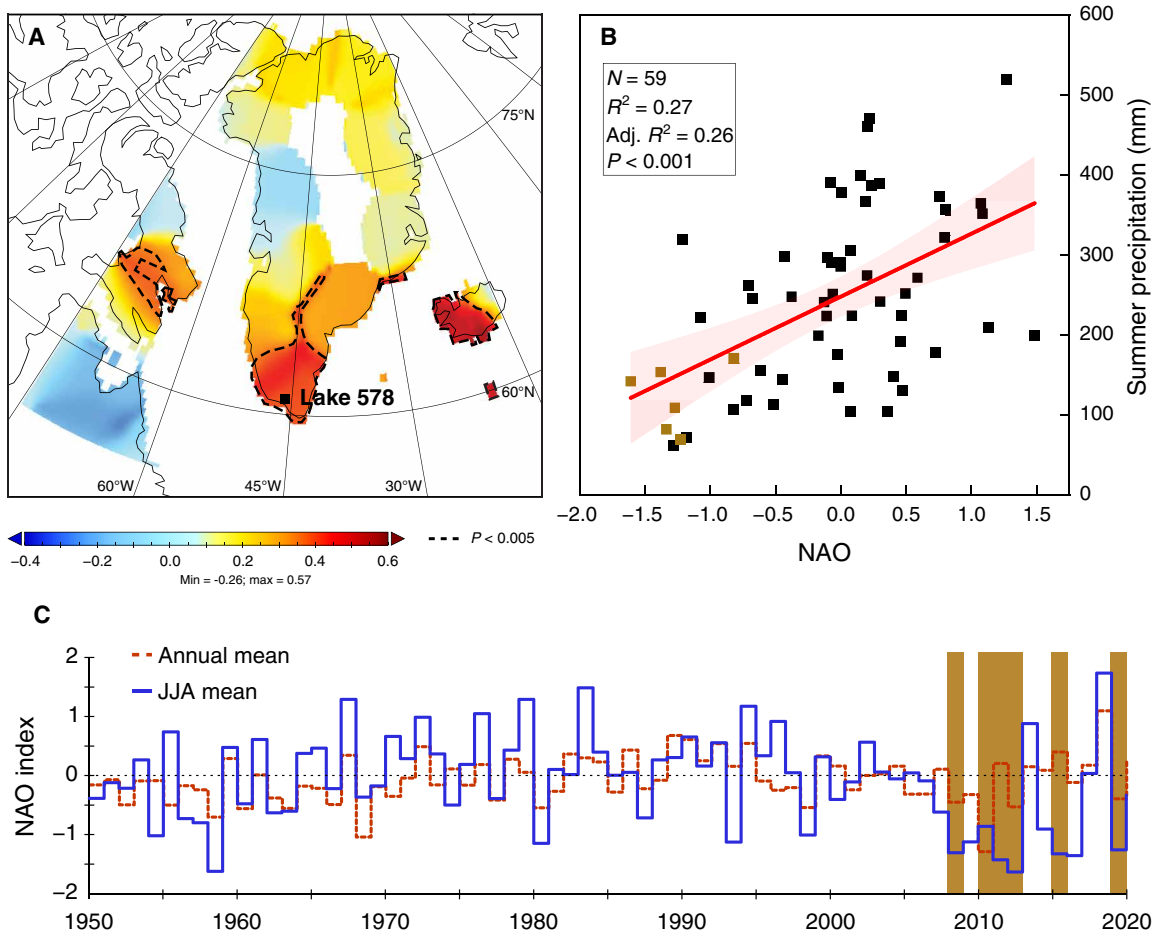


**Fig. 3. NAO in southern Greenland and its connection to summer precipitation [June, July, and August (JJA)].** (**A**) Spatial correlation between summer NAO and precipitation from 1950 to 2020; dashed lines include areas of significant correlations ($P < 0.005$). The precipitation data are based on the CRU TS 4.04 precipitation dataset from the Climate Explorer (climexp.knmi.nl). (**B**) The correlation between summer NAO and measured precipitation from the Narsarsuaq weather station (1961–2020) (fig. S1B). The red line is the linear fit, and the shaded area represents the 95% CI. (**C**) Time series of the annual mean and JJA mean NAO index plotted from 1950 to 2020. Brown columns [corresponding to brown squares in (B)] indicate recently observed and documented summer droughts that led to a notable decrease in grass, crop, and hay production (*15*). NAO index in all figures is excerpted from the "NAO (rotated EOF of Z500, 1950-now, CPC)" dataset from the Climate Explorer (climexp.knmi.nl).

of hay and silage, which was characterized as a national problem (*14*). Because of a lack of precipitation, a substantial hay yield decline occurred in the following years of 2010, 2011, 2012, and 2015 (*15*). All these severe drought summers (including 2019) had concurrent negative summer NAO, and they were the most anomalous in the past 70 years (Fig. 3C). While today, such conditions can be ameliorated by importing hay, that option was not available to the Norse settlers, who were increasingly vulnerable to the persistently drier conditions. We acknowledge that the causes of Norse settlement abandonment are complex, and it is difficult to simply attribute them exclusively to climate change. Nevertheless, our results highlight that the hydroclimate changes were tightly tied to the destiny of the Eastern Settlement.

## MATERIALS AND METHODS

### Field sampling

We collected a 70-cm sediment core from Lake 578 (61°50′ N, 45°37′ W) in July 2016, using a UWITEC (Austria) gravity corer with a percussion hammer. Terrestrial and aquatic plant samples were obtained in July 2017. Lake water samples were collected in July 2018. All samples were shipped back to the University of Massachusetts Amherst. The sediment core was stored in a dark cold room (4°C) until analysis. Plant samples were frozen until analysis. Water samples were stored in a refrigerator until analysis. For more details, see the Supplementary Materials.

### Age-depth model

The age-depth model of Lake 578 sediment core is developed on the basis of radiometric dating. The upper 15 cm of sediment core was subsampled at 1-cm resolution in the field. The $^{210}$Pb, $^{214}$Pb, and $^{137}$Cs activity of these 15 samples was measured using Canberra GL2020R Low Energy Germanium Detector at the University of Massachusetts Amherst. Seven discrete terrestrial macrofossils were collected from the sediment core, and radiocarbon analysis was conducted in W.M. Keck Carbon Cycle Accelerator Mass Spectrometer at the University of California, Irvine. Radiocarbon age estimates were calibrated using the "IntCal20" calibration in the R program "BChron." For more details, see the Supplementary Materials.

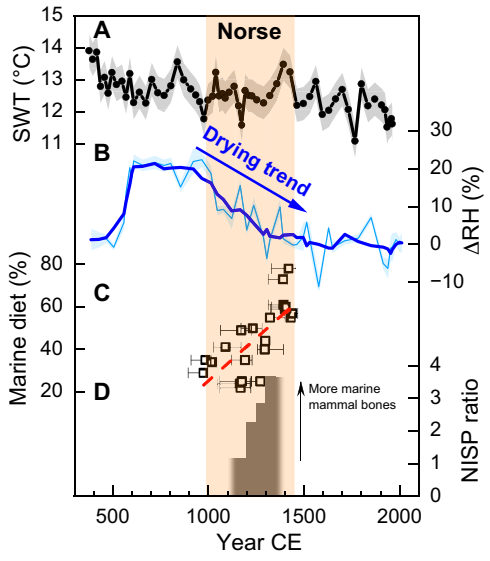


**Fig. 4. The reconstructed climate conditions from southern Greenland and the Norse diet transition.** (**A**) BrGDGT-inferred summer water temperature (SWT) from southern Greenland. An error bar of ±0.52°C from the calibration (*19*) is shown with the gray shading. (**B**) Leaf wax hydrogen isotope-inferred ΔRH from southern Greenland. Blue shading represents the 90% CI. The thick blue line represents 5-point running mean. (**C**) Percentage of marine sourced food in the Norse diet (*46*). (**D**) The ratio of marine to terrestrial mammal bones [number of identified specimens (NISP)] from a Norse farm in Qassiarsuk (*47*). Orange bar indicates the time span of Norse settlement.

### Lipid biomarker analysis

Sediments at 1-cm resolution were freeze dried and homogenized. The total lipid extract (TLE) was acquired using a Dionex Accelerated Solvent Extractor 200 with a solvent mixture of dichloromethane and methanol (MeOH) (9:1, v/v). The TLE was further separated into apolar, ketone, and polar fractions with alumina oxide column chromatography.

To measure brGDGTs, the polar fractions were dissolved in hexane/isopropanol (99:1, v/v) and filtered through 0.45-μm polytetrafluoroethylene (PTFE) syringe filters. A known amount of $C_{46}$ GDGT internal standard was added to each sample to quantify the brGDGT concentrations. Subsequently, all samples were analyzed using an Agilent 1260 high-performance liquid chromatography coupled to an Agilent 6120 Quadrupole mass selective detector with a method (*49*) that can differentiate the 5- and 6-methyl isomers. Mass scanning was conducted in selected ion monitoring mode for mass/charge ratios of 1302, 1300, 1298, 1296, 1292, 1050, 1048, 1046, 1036, 1034, 1032, 1022, 1020, 1018, and 744.

To measure leaf wax hydrogen isotopes, all apolar fractions were purified with silver nitrate silica gel chromatography, and the *n*-alkane concentrations were determined using a gas chromatograph (GC) equipped with a flame ionization detector. As the *n*-alkane concentrations of the 1-cm interval samples were generally low, we combined every two adjacent samples yielding 35 isotopic measurements. An additional 11 samples from ~600, ~1000, and ~1400 CE were processed following an identical protocol to increase the resolution of the reconstruction in key time intervals. The $\delta^2H$ of $C_{23}$, $C_{25}$, $C_{27}$, and $C_{29}$ *n*-alkanes for a total of 46 samples were measured on Thermo Delta V Advantage isotope ratio mass spectrometer coupled to a Thermo Trace GC Ultra through a GCC III. All samples were measured in triplicate, bracketed by two or three injections of $H_2$ reference gas, with laboratory internal standards injections between each sample and three times at the beginning and end of each sequence, to track and correct intersample drift. Sample $\delta^2H$ ratios are expressed in per mil (‰) relative to Vienna Standard Mean Ocean Water (VSMOW). The complete methods are detailed in the Supplementary Materials.

## SUPPLEMENTARY MATERIALS

Supplementary material for this article is available at https://science.org/doi/10.1126/sciadv.abm4346

## REFERENCES AND NOTES


1. T. H. McGovern, in *The Anthropology of Climate Change: An historical reader* (2014), pp. 131–150.
2. G. Jones, *The Norse Atlantic saga: Being the Norse voyages of discovery and settlement to Iceland, Greenland, and North America* (Oxford Univ. Press, USA, 1986).
3. J. Arneborg, N. Lynnerup, J. Heinemeier, Human diet and subsistence patterns in Norse Greenland AD c.980—AD c.1450: Archaeological interpretations. *J. North Atl.* **301**, 119–133 (2012).
4. N. Lynnerup, Paleodemography of the Greenland Norse. *Arctic Anthropol.* **33**, 122–136 (1996).
5. A. J. Dugmore, T. H. McGovern, O. Vésteinsson, J. Arneborg, R. Streeter, C. Keller, Cultural adaptation, compounding vulnerabilities and conjunctures in Norse Greenland. *Proc. Natl. Acad. Sci. U.S.A.* **109**, 3658–3663 (2012).
6. W. J. D'Andrea, Y. Huang, S. C. Fritz, N. J. Anderson, Abrupt Holocene climate change as an important factor for human migration in West Greenland. *Proc. Natl. Acad. Sci. U.S.A.* **108**, 9765–9769 (2011).
7. J. Berglund, The decline of the Norse Settlements in Greenland. *Arctic Anthropol.* **23**, 109–135 (1986).
8. L. Millet, C. Massa, V. Bichet, V. Frossard, S. Belle, E. Gauthier, Anthropogenic versus climatic control in a high-resolution 1500-year chironomid stratigraphy from a southwestern Greenland lake. *Quat. Res.* **81**, 193–202 (2014).
9. K. G. Jensen, A. Kuijpers, N. Koç, J. Heinemeier, Diatom evidence of hydrographic changes and ice conditions in Igaliku Fjord, South Greenland, during the past 1500 years. *Holocene* **14**, 152–164 (2004).
10. C. S. Andresen, S. Björck, O. Bennike, G. Bond, Holocene climate changes in southern Greenland: Evidence from lake sediments. *J. Quat. Sci.* **19**, 783–795 (2004).
11. G. E. Lasher, Y. Axford, Medieval warmth confirmed at the Norse Eastern Settlement in Greenland. *Geology* **47**, 267–270 (2019).
12. C. Massa, B. B. Perren, É. Gauthier, V. Bichet, C. Petit, H. Richard, A multiproxy evaluation of Holocene environmental change from Lake Igaliku, South Greenland. *J. Paleolimnol.* **48**, 241–258 (2012).
13. M. R. Kaplan, A. P. Wolfe, G. H. Miller, Holocene environmental variability in southern Greenland inferred from lake sediments. *Quatern. Res.* **58**, 149–159 (2002).
14. E. de Neergaard, P. Stougaard, K. Høegh, L. Munk, Climatic changes and agriculture in Greenland: Plant diseases in potatoes and grass fields. *IOP Conf. Ser. Earth Environ. Sci.* **6**, 372013 (2009).
15. C. Caviezel, M. Hunziker, N. J. Kuhn, Bequest of the Norseman—The potential for agricultural intensification and expansion in southern Greenland under climate change. *Land.* **6**, 87 (2017).
16. T. A. Halamka, J. M. McFarlin, A. D. Younkin, J. Depoy, N. Dildar, S. H. Kopf, Oxygen limitation can trigger the production of branched GDGTs in culture. *Geochemical Perspect. Lett.* **19**, 36–39 (2021).
17. J. W. H. Weijers, S. Schouten, J. C. van den Donker, E. C. Hopmans, J. S. Sinninghe Damsté, Environmental controls on bacterial tetraether membrane lipid distribution in soils. *Geochim. Cosmochim. Acta* **71**, 703–713 (2007).
18. C. De Jonge, E. C. Hopmans, C. I. Zell, J. H. Kim, S. Schouten, J. S. Sinninghe Damsté, Occurrence and abundance of 6-methyl branched glycerol dialkyl glycerol tetraethers in soils: Implications for palaeoclimate reconstruction. *Geochim. Cosmochim. Acta* **141**, 97–112 (2014).
19. B. Zhao, I. S. Castañeda, R. S. Bradley, J. M. Salacup, G. A. de Wet, W. C. Daniels, T. Schneider, Development of an in situ branched GDGT calibration in Lake 578, southern Greenland. *Org. Geochem.* **152**, 104168 (2021).
20. D. S. Kaufman, D. P. Schneider, N. P. McKay, C. M. Ammann, R. S. Bradley, K. R. Briffa, G. H. Miller, B. L. Otto-Bliesner, J. T. Overpeck, B. M. Vinther, M. Abbott, Y. Axford, B. Bird, H. J. B. Birks, A. E. Bjune, J. Briner, T. Cook, M. Chipman, P. Francus, K. Gajewski, A. Geirsdottir, F. S. Hu, B. Kutchko, S. Lamoureux, M. Loso, G. MacDonald, M. Peros,

D. Porinchu, C. Schiff, H. Seppa, E. Thomas, Recent warming reverses long-term Arctic cooling. *Science* **325**, 1236–1239 (2009).
21. J. Laskar, P. Robutel, F. Joutel, M. Gastineau, A. C. M. Correia, B. Levrard, A long-term numerical solution for the insolation quantities of the Earth. *Astron. Astrophys.* **428**, 261–285 (2004).
22. N. K. Larsen, J. Find, A. Kristensen, A. A. Bjørk, K. K. Kjeldsen, B. V. Odgaard, J. Olsen, K. H. Kjær, Holocene ice marginal fluctuations of the Qassimiut lobe in South Greenland. *Sci. Rep.* **6**, 22362 (2016).
23. K. Winsor, A. E. Carlson, D. H. Rood, $^{10}$Be dating of the Narsarsuaq moraine in southernmost Greenland: Evidence for a late-Holocene ice advance exceeding the Little Ice Age maximum. *Quat. Sci. Rev.* **98**, 135–143 (2014).
24. A. Miettinen, D. V. Divine, K. Husum, N. Koç, A. Jennings, Exceptional ocean surface conditions on the SE Greenland shelf during the Medieval Climate Anomaly. *Paleoceanography* **30**, 1657–1674 (2015).
25. A. Miettinen, D. Divine, N. Kocx, F. Godtliebsen, I. R. Hall, Multicentennial variability of the sea surface temperature gradient across the subpolar North Atlantic over the last 2.8 kyr. *J. Climate* **25**, 4205–4219 (2012).
26. J. P. Briner, N. P. McKay, Y. Axford, O. Bennike, R. S. Bradley, A. de Vernal, D. Fisher, P. Francus, B. Fréchette, K. Gajewski, A. Jennings, D. S. Kaufman, G. Miller, C. Rouston, B. Wagner, Holocene climate change in Arctic Canada and Greenland. *Quat. Sci. Rev.* **147**, 340–364 (2016).
27. Y. Axford, A. De Vernal, E. C. Osterberg, Past warmth and its impacts during the Holocene thermal maximum in Greenland. *Annu. Rev. Earth Planet. Sci.* **49**, 279–307 (2021).
28. G. Eglinton, R. J. Hamilton, Leaf epicuticular waxes. *Science* **156**, 1322–1335 (1967).
29. K. J. Ficken, B. Li, D. L. Swain, G. Eglinton, An n-alkane proxy for the sedimentary input of submerged/floating freshwater aquatic macrophytes. *Org. Geochem.* **31**, 745–749 (2000).
30. A. L. Sessions, T. W. Burgoyne, A. Schimmelmann, J. M. Hayes, Fractionation of hydrogen isotopes in lipid biosynthesis. *Org. Geochem.* **30**, 1193–1200 (1999).
31. O. Rach, A. Kahmen, A. Brauer, D. Sachse, A dual-biomarker approach for quantification of changes in relative humidity from sedimentary lipid D/H ratios. *Clim. Past.* **13**, 741–757 (2017).
32. E. K. Thomas, I. S. Castañeda, N. P. McKay, J. P. Briner, J. M. Salacup, K. Q. Nguyen, A. D. Schweinsberg, The Wetter Arctic coincident with hemispheric warming 8,000 years ago. *Geophys. Res. Lett.* **45**, 10637–10647 (2018).
33. H. Dion-Kirschner, J. M. McFarlin, A. L. Masterson, Y. Axford, M. R. Osburn, Modern constraints on the sources and climate signals recorded by sedimentary plant waxes in west Greenland. *Geochim. Cosmochim. Acta* **286**, 336–354 (2020).
34. B. M. Vinther, S. L. Buchardt, H. B. Clausen, D. Dahl-Jensen, S. J. Johnsen, D. A. Fisher, R. M. Koerner, D. Raynaud, V. Lipenkov, K. K. Andersen, T. Blunier, S. O. Rasmussen, J. P. Steffensen, A. M. Svensson, Holocene thinning of the Greenland ice sheet. *Nature* **461**, 385–388 (2009).
35. M. B. Osman, B. E. Smith, L. D. Trusel, S. B. Das, J. R. McConnell, N. Chellman, M. Arienzo, H. Sodemann, Abrupt Common Era hydroclimate shifts drive west Greenland ice cap change. *Nat. Geosci.* **14**, 756–761 (2021).
36. J. W. Hurrell, Decadal trends in the North Atlantic oscillation: Regional temperatures and precipitation. *Science* **269**, 676–679 (1995).
37. J. W. Hurrell, M. P. Hoerling, C. K. Folland, in *International Geophysics* (2002; https://linkinghub.elsevier.com/retrieve/pii/S0074614202801632), vol. 83, pp. 143–151.
38. E. Hanna, T. E. Cropper, R. J. Hall, J. Cappelen, Greenland blocking index 1851–2015: A regional climate change signal. *Int. J. Climatol.* **36**, 4847–4861 (2016).
39. J. Olsen, N. J. Anderson, M. F. Knudsen, Variability of the North Atlantic Oscillation over the past 5,200 years. *Nat. Geosci.* **5**, 808–812 (2012).
40. V. Trouet, J. Esper, N. E. Graham, A. Baker, J. D. Scourse, D. C. Frank, Persistent positive North Atlantic Oscillation mode dominated the medieval climate anomaly. *Science* **324**, 78–80 (2009).
41. P. Ortega, F. Lehner, D. Swingedouw, V. Masson-Delmotte, C. C. Raible, M. Casado, P. Yiou, A model-tested North Atlantic Oscillation reconstruction for the past millennium. *Nature* **523**, 71–74 (2015).
42. R. Zhang, R. Sutton, G. Danabasoglu, Y. O. Kwon, R. Marsh, S. G. Yeager, D. E. Amrhein, C. M. Little, A review of the role of the Atlantic meridional overturning circulation in atlantic multidecadal variability and associated climate impacts. *Rev. Geophys.* **57**, 316–375 (2019).
43. M. B. Osman, S. Coats, S. B. Das, J. R. McConnell, N. Chellman, North Atlantic jet stream projections in the context of the past 1,250 years. *Proc. Natl. Acad. Sci. U.S.A.* **118**, e2104105118 (2021).
44. P. C. Buckland, K. J. Edwards, E. Panagiotakopulu, J. E. Schofield, Palaeoecological and historical evidence for manuring and irrigation at Garðar (Igaliku), Norse Eastern Settlement, Greenland. *Holocene* **19**, 105–116 (2009).
45. K. J. Edwards, J. E. Schofield, Investigation of proposed Norse irrigation channels and dams at Garðar/Igaliku, Greenland. *Water Hist.* **5**, 71–92 (2013).
46. J. Arneborg, J. Heinemeier, N. Lynnerup, H. L. Nielsen, N. Rud, Change of diet of the Greenland Vikings determined from stable carbon isotope analysis and $^{14}$C dating of their bones. *Radiocarbon* **41**, 157–168 (1999).
47. T. H. McGovern, A. Palsdóttir, Preliminary report of a Medieval Norse Archaeofauna from Brattahlið North Farm (KNK 2629), Qassiarsuk, Greenland. *Natl. Geogr. Mag.* , 1–22 (2006).
48. T. H. McGovern, Causation in Norse Greenland. *Artic Antropol.* **28**, 77–100 (2016).
49. E. C. Hopmans, S. Schouten, J. S. Sinninghe Damsté, The effect of improved chromatography on GDGT-based palaeoproxies. *Org. Geochem.* **93**, 1–6 (2016).
50. E. Kokfelt, T.F., Weng, W.L., Willerslev, *Geological map of South and South West Greenland - 1 : 100 000, February 2019* (Copenhagen: Geological Survey of Denmark and Greenland, 2019; https://eng.geus.dk/about/news/news-archive/2019/mar/new-geological-map-of-south-and-south-west-greenland).
51. J. Nusbaumer, P. M. Alexander, A. N. LeGrande, M. Tedesco, Spatial shift of greenland moisture sources related to enhanced arctic warming. *Geophys. Res. Lett.* **46**, 14723–14731 (2019).
52. A. A. Cluett, E. K. Thomas, S. M. Evans, P. W. Keys, Seasonal variations in moisture origin explain spatial contrast in precipitation isotope seasonality on coastal western Greenland. *J. Geophys. Res. Atmos.* **126**, 1–15 (2021).
53. O. Heiri, A. F. Lotter, G. Lemcke, Loss on ignition as a method for estimating organic and carbonate content in sediments: Reproducibility and comparability of results. *J. Paleolimnol.* **25**, 101–110 (2001).
54. J. Walter, E. Dean, Determination of carbonate and organic matter in calcareous sediments and sedimentary rocks by loss on ignition: Comparison with other methods. *SEPM J. Sediment. Res.* **44**, 242–248 (1974).
55. J. D. Woodruff, A. P. Martini, E. Z. H. Elzidani, T. J. Naughton, D. J. Kekacs, D. G. MacDonald, Off-river waterbodies on tidal rivers: Human impact on rates of infilling and the accumulation of pollutants. *Geomorphology* **184**, 38–50 (2013).
56. P. G. Appleby, F. Oldfield, The calculation of lead-210 dates assuming a constant rate of supply of unsupported 210Pb to the sediment. *Catena* **5**, 1–8 (1978).
57. P. G. Appleby, Three decades of dating recent sediments by fallout radionuclides: A review. *Holocene* **18**, 83–93 (2008).
58. J. Carroll, I. Lerche, *Sedimentary Processes: Quantification Using Radionuclides* (Elsevier, 2003).
59. W. Tylmann, D. Enters, M. Kinder, P. Moska, C. Ohlendorf, G. Poręba, B. Zolitschka, Multiple dating of varved sediments from Lake Łazduny, northern Poland: Toward an improved chronology for the last 150 years. *Quat. Geochronol.* **15**, 98–107 (2013).
60. L. von Gunten, M. Grosjean, J. Beer, P. Grob, A. Morales, R. Urrutia, Age modeling of young non-varved lake sediments: Methods and limits. Examples from two lakes in Central Chile. *J. Paleolimnol.* **42**, 401–412 (2009).
61. P. J. Reimer, W. E. N. Austin, E. Bard, A. Bayliss, P. G. Blackwell, C. B. Ramsey, M. Butzin, H. Cheng, R. L. Edwards, M. Friedrich, P. M. Grootes, T. P. Guilderson, I. Hajdas, T. J. Heaton, A. G. Hogg, K. A. Hughen, B. Kromer, S. W. Manning, R. Muscheler, J. G. Palmer, C. Pearson, J. van der Plicht, R. W. Reimer, D. A. Richards, E. M. Scott, J. R. Southon, C. S. M. Turney, L. Wacker, F. Adolphi, U. Büntgen, M. Capano, S. M. Fahrni, A. Fogtmann-Schulz, R. Friedrich, P. Köhler, S. Kudsk, F. Miyake, J. Olsen, F. Reinig, M. Sakamoto, A. Sookdeo, S. Talamo, The IntCal20 Northern Hemisphere radiocarbon age calibration curve (0–55 cal kBP). *Radiocarbon* **62**, 725–757 (2020).
62. J. Haslett, A. Parnell, A simple monotone process with application to radiocarbon-dated depth chronologies. *J. R. Stat. Soc. Ser. C (Applied Stat.)* **57**, 399–418 (2008).
63. J. S. Sinninghe Damsté, E. C. Hopmans, R. D. Pancost, S. Schouten, J. A. J. Geenevasen, Newly discovered non-isoprenoid glycerol dialkyl glycerol tetraether lipids in sediments. *Chem. Commun.* **2000**, 1683–1684 (2000).
64. S. Schouten, E. C. Hopmans, J. S. Sinninghe Damsté, The organic geochemistry of glycerol dialkyl glycerol tetraether lipids: A review. *Org. Geochem.* **54**, 19–61 (2013).
65. J. S. Sinninghe Damsté, W. I. C. Rijpstra, B. U. Foesel, K. J. Huber, J. Overmann, S. Nakagawa, J. J. Kim, P. F. Dunfield, S. N. Dedysh, L. Villanueva, An overview of the occurrence of ether- and ester-linked iso-diabolic acid membrane lipids in microbial cultures of the Acidobacteria: Implications for brGDGT paleoproxies for temperature and pH. *Org. Geochem.* **124**, 63–76 (2018).
66. F. Peterse, J. van der Meer, S. Schouten, J. W. H. Weijers, N. Fierer, R. B. Jackson, J.-H. Kim, J. S. Sinninghe Damsté, Revised calibration of the MBT–CBT paleotemperature proxy based on branched tetraether membrane lipids in surface soils. *Geochim. Cosmochim. Acta* **96**, 215–229 (2012).
67. B. D. A. Naafs, A. V. Gallego-Sala, G. N. Inglis, R. D. Pancost, Refining the global branched glycerol dialkyl glycerol tetraether (brGDGT) soil temperature calibration. *Org. Geochem.* **106**, 48–56 (2017).
68. B. D. A. Naafs, G. N. Inglis, Y. Zheng, M. J. Amesbury, H. Biester, R. Bindler, J. Blewett, M. A. Burrows, D. del Castillo Torres, F. M. Chambers, A. D. Cohen, R. P. Evershed, S. J. Feakins, M. Gałka, A. Gallego-Sala, L. Gandois, D. M. Gray, P. G. Hatcher, E. N. H. Coronado, P. D. M. Hughes, A. Huguet, M. Könönen, F. Laggoun-Défarge, O. Lähteenoja, M. Lamentowicz, R. Marchant, E. McClymont, X. Pontevedra-Pombal,

C. Ponton, A. Pourmand, A. M. Rizzuti, L. Rochefort, J. Schellekens, F. De Vleeschouwer, R. D. Pancost, Introducing global peat-specific temperature and pH calibrations based on brGDGT bacterial lipids. *Geochim. Cosmochim. Acta* **208**, 285–301 (2017).
69. E. Dearing Crampton-Flood, J. E. Tierney, F. Peterse, F. M. S. A. Kirkels, J. S. Sinninghe Damsté, BayMBT: A Bayesian calibration model for branched glycerol dialkyl glycerol tetraethers in soils and peats. *Geochim. Cosmochim. Acta* **268**, 142–159 (2020).
70. C. De Jonge, D. Radujković, B. D. Sigurdsson, J. T. Weedon, I. Janssens, F. Peterse, Lipid biomarker temperature proxy responds to abrupt shift in the bacterial community composition in geothermally heated soils. *Org. Geochem.* **137**, 103897 (2019).
71. J. M. Russell, E. C. Hopmans, S. E. Loomis, J. Liang, J. S. Sinninghe Damsté, Distributions of 5- and 6-methyl branched glycerol dialkyl glycerol tetraethers (brGDGTs) in East African lake sediment: Effects of temperature, pH, and new lacustrine paleotemperature calibrations. *Org. Geochem.* **117**, 56–69 (2018).
72. X. Dang, W. Ding, H. Yang, R. D. Pancost, B. D. A. Naafs, J. Xue, X. Lin, J. Lu, S. Xie, Different temperature dependence of the bacterial brGDGT isomers in 35 Chinese lake sediments compared to that in soils. *Org. Geochem.* **119**, 72–79 (2018).
73. J. Raberg, D. Harning, S. Crump, G. de Wet, A. Blumm, S. Kopf, Á. Geirsdóttir, G. Miller, J. Sepúlveda, Revised fractional abundances and warm-season temperatures substantially improve brGDGT calibrations in lake sediments. *Biogeosciences* **18**, 3579–3603 (2021).
74. P. Martínez-Sosa, J. E. Tierney, I. C. Stefanescu, E. Dearing Crampton-Flood, B. N. Shuman, C. Routson, A global Bayesian temperature calibration for lacustrine brGDGTs. *Geochim. Cosmochim. Acta* **305**, 87–105 (2021).
75. G. A. de Wet, I. S. Castañeda, R. M. DeConto, J. Brigham-Grette, A high-resolution mid-Pleistocene temperature record from Arctic Lake El'gygytgyn: A 50 kyr super interglacial from MIS 33 to MIS 31? *Earth Planet. Sci. Lett.* **436**, 56–63 (2016).
76. I. C. Stefanescu, B. N. Shuman, J. E. Tierney, Temperature and water depth effects on brGDGT distributions in sub-alpine lakes of mid-latitude North America. *Org. Geochem.* **152**, 104174 (2021).
77. D. Dahl-Jensen, K. Mosegaard, N. Gundestrup, G. D. Clow, S. J. Johnsen, A. W. Hansen, N. Balling, Past temperatures directly from the Greenland ice sheet. *Science* **282**, 268–271 (1998).
78. J. Hou, Y. Huang, Y. Wang, B. Shuman, W. W. Oswald, E. Faison, D. R. Foster, Postglacial climate reconstruction based on compound-specific D/H ratios of fatty acids from Blood Pond, New England. *Geochemistry, Geophys. Geosystems.* **7**, 1–11 (2006).
79. L. Gao, J. Hou, J. Toney, D. MacDonald, Y. Huang, Mathematical modeling of the aquatic macrophyte inputs of mid-chain n-alkyl lipids to lake sediments: Implications for interpreting compound specific hydrogen isotopic records. *Geochim. Cosmochim. Acta* **75**, 3781–3791 (2011).
80. J. E. Nichols, M. Walcott, R. Bradley, J. Pilcher, Y. Huang, Quantitative assessment of precipitation seasonality and summer surface wetness using ombrotrophic sediments from an Arctic Norwegian peatland. *Quatern. Res.* **72**, 443–451 (2009).
81. R. T. Bush, F. A. McInerney, Leaf wax n-alkane distributions in and across modern plants: Implications for paleoecology and chemotaxonomy. *Geochim. Cosmochim. Acta* **117**, 161–179 (2013).
82. C. Massa, V. Bichet, E. Gauthier, B. B. Perren, O. Mathieu, C. Petit, F. Monna, J. Giraudeau, R. Losno, H. Richard, A 2500 year record of natural and anthropogenic soil erosion in South Greenland. *Quat. Sci. Rev.* **32**, 119–130 (2012).
83. V. Bichet, E. Gauthier, C. Massa, B. B. Perren, Lake sediments as an archive of land use and environmental change in the eastern settlement, Southwestern Greenland. *J. North Atl.* **601**, 47–63 (2014).
84. B. Aichner, S. Hilt, C. Périllon, M. Gillefalk, D. Sachse, Biosynthetic hydrogen isotopic fractionation factors during lipid synthesis in submerged aquatic macrophytes: Effect of groundwater discharge and salinity. *Org. Geochem.* **113**, 10–16 (2017).
85. Y. Huang, B. Shuman, Y. Wang, T. Webb, Hydrogen isotope ratios of individual lipids in lake sediments as novel tracers of climatic and environmental change: A surface sediment test. *J. Paleolimnol.* **31**, 363–375 (2004).
86. D. Sachse, J. Radke, G. Gleixner, Hydrogen isotope ratios of recent lacustrine sedimentary n-alkanes record modern climate variability. *Geochim. Cosmochim. Acta* **68**, 4877–4889 (2004).
87. B. Aichner, U. Herzschuh, H. Wilkes, A. Vieth, J. Böhner, δD values of n-alkanes in Tibetan lake sediments and aquatic macrophytes—A surface sediment study and application to a 16ka record from Lake Koucha. *Org. Geochem.* **41**, 779–790 (2010).
88. J. Hou, W. J. D'Andrea, D. MacDonald, Y. Huang, Hydrogen isotopic variability in leaf waxes among terrestrial and aquatic plants around Blood Pond, Massachusetts (USA). *Org. Geochem.* **38**, 977–984 (2007).
89. O. Rach, A. Brauer, H. Wilkes, D. Sachse, Delayed hydrological response to Greenland cooling at the onset of the Younger Dryas in western Europe. *Nat. Geosci.* **7**, 109–112 (2014).
90. C. E. Jonsson, M. J. Leng, G. C. Rosqvist, J. Seibert, C. Arrowsmith, Stable oxygen and hydrogen isotopes in sub-Arctic lake waters from northern Sweden. *J. Hydrol.* **376**, 143–151 (2009).
91. A. A. Cluett, E. K. Thomas, Resolving combined influences of inflow and evaporation on western Greenland lake water isotopes to inform paleoclimate inferences. *J. Paleolimnol.* **63**, 251–268 (2020).
92. E. K. Thomas, K. V. Hollister, A. A. Cluett, M. C. Corcoran, Reconstructing Arctic precipitation seasonality using aquatic leaf wax $\delta^2$H in lakes with contrasting residence times. *Paleoceanogr. Paleoclimatology.* **35**, 1–19 (2020).
93. G. J. Bowen, J. Revenaugh, Interpolating the isotopic composition of modern meteoric precipitation. *Water Resour. Res.* **39**, 1–13 (2003).
94. B. Shuman, Y. Huang, P. Newby, Y. Wang, Compound-specific isotopic analyses track changes in seasonal precipitation regimes in the Northeastern United States at ca 8200 cal yr BP. *Quat. Sci. Rev.* **25**, 2992–3002 (2006).
95. E. K. Thomas, J. P. Briner, J. J. Ryan-Henry, Y. Huang, A major increase in winter snowfall during the middle Holocene on western Greenland caused by reduced sea ice in Baffin Bay and the Labrador Sea. *Geophys. Res. Lett.* **43**, 5302–5308 (2016).
96. K. F. O'Connor, M. A. Berke, L. A. Ziolkowski, Hydrogen isotope fractionation in modern plants along a boreal-tundra transect in Alaska. *Org. Geochem.* **147**, 104064 (2020).
97. W. C. Daniels, J. M. Russell, A. E. Giblin, J. M. Welker, E. S. Klein, Y. Huang, Hydrogen isotope fractionation in leaf waxes in the Alaskan Arctic tundra. *Geochim. Cosmochim. Acta* **213**, 216–236 (2017).
98. M. A. Berke, A. Cartagena Sierra, R. Bush, D. Cheah, K. O'Connor, Controls on leaf wax fractionation and δ2H values in tundra vascular plants from western Greenland. *Geochim. Cosmochim. Acta* **244**, 565–583 (2019).
99. A. Kahmen, E. Schefuß, D. Sachse, Leaf water deuterium enrichment shapes leaf wax n-alkane δd values of angiosperm plants I: Experimental evidence and mechanistic insights. *Geochim. Cosmochim. Acta* **111**, 39–49 (2013).
100. L. Curtin, W. J. D'Andrea, N. Balascio, G. Pugsley, G. de Wet, R. Bradley, Holocene and Last Interglacial climate of the Faroe Islands from sedimentary plant wax hydrogen and carbon isotopes. *Quat. Sci. Rev.* **223**, 105930 (2019).
101. T. E. Arnold, A. F. Diefendorf, M. Brenner, K. H. Freeman, A. A. Baczynski, Climate response of the Florida Peninsula to Heinrich events in the North Atlantic. *Quat. Sci. Rev.* **194**, 1–11 (2018).
102. J. L. Toney, A. García-Alix, G. Jiménez-Moreno, R. S. Anderson, H. Moossen, O. Seki, New insights into Holocene hydrology and temperature from lipid biomarkers in western Mediterranean alpine wetlands. *Quat. Sci. Rev.* **240**, 106395 (2020).
103. D. Sachse, I. Billault, G. J. Bowen, Y. Chikaraishi, T. E. Dawson, S. J. Feakins, K. H. Freeman, C. R. Magill, F. A. McInerney, M. T. J. van der Meer, P. Polissar, R. J. Robins, J. P. Sachs, H.-L. Schmidt, A. L. Sessions, J. W. C. White, J. B. West, A. Kahmen, Molecular paleohydrology: Interpreting the hydrogen-isotopic composition of lipid biomarkers from photosynthesizing organisms. *Annu. Rev. Earth Planet. Sci.* **40**, 221–249 (2012).
104. H. Jacob, C. Sonntag, An 8-year record of the seasonal variation of $^2$H and $^{18}$O in atmospheric water vapour and precipitation at Heidelberg, Germany. *Germany. Tellus B.* **43**, 291–300 (1991).
105. D. F. Boutt, S. B. Mabee, Q. Yu, Multiyear increase in the stable isotopic composition of stream water from groundwater recharge due to extreme precipitation. *Geophys. Res. Lett.* **46**, 5323–5330 (2019).
106. L. von Gunten, M. Grosjean, B. Rein, R. Urrutia, P. Appleby, A quantitative high-resolution summer temperature reconstruction based on sedimentary pigments from Laguna Aculeo, central Chile, back to AD 850. *Holocene* **19**, 873–881 (2009).
107. H. N. Dunning, Geochemistry of organic pigments. *Org. Geochem.* , 367–430 (1963).
108. T. Schneider, D. Rimer, C. Butz, M. Grosjean, A high-resolution pigment and productivity record from the varved Ponte Tresa basin (Lake Lugano, Switzerland) since 1919: Insight from an approach that combines hyperspectral imaging and high-performance liquid chromatography. *J. Paleolimnol.* **60**, 381–398 (2018).
109. C. Butz, M. Grosjean, T. Goslar, W. Tylmann, Hyperspectral imaging of sedimentary bacterial pigments: A 1700-year history of meromixis from varved Lake Jaczno, northeast Poland. *J. Paleolimnol.* **58**, 57–72 (2017).
110. B. Rein, F. Sirocko, In-situ reflectance spectroscopy—Analysing techniques for high-resolution pigment logging in sediment cores. *Int. J. Earth Sci.* **91**, 950–954 (2002).
111. R. Schlitzer, Ocean data view (2018); https://odv.awi.de/.
112. N. Mikkelsen, A. Kuijpers, Marine and terrestrial investigations in the Norse Eastern Settlement, south Greenland. *Geol. Greenl. Surv. Bull.* **189**, 65–69 (2001).
113. C. Porter, P. Morin, I. Howat, M.-J. Noh, B. Bates, K. Peterman, S. Keesey, M. Schlenk, J. Gardiner, K. Tomko, ArcticDEM. *Harvard Dataverse.* **1**, 2018–2030 (2018).

**Acknowledgments:** We thank the editor and two anonymous reviewers for their comments that helped improve this paper. We thank E. Jensen and H. Knudsen (Sillisit, Greenland) for letting us conduct fieldwork on their land, for assistance with field logistics, and for sharing knowledge of traditional Greenland farming practices with us. We also thank D. Miller, A. de Wet, J. Brush, R. Meyer, and J. Daniels for fieldwork assistance. **Funding:** U.S. National Science

Foundation OPP-1602973 (R.S.B. and I.S.C.), UMass Amherst Geoscience Alumni Research Awards (B.Z.), The Geological Society of America Graduate Student Research Grants (B.Z.), SNSF Early Postdoc Mobility fellowship #184428 (T.S.), NSF EAR-IF grant #1652274 (E.K.T.), and The College of Natural Sciences, University of Massachusetts Amherst. **Author contributions:** Conceptualization: I.S.C., R.S.B., and B.Z. Methodology: B.Z., I.S.C., E.K.T., and R.S.B. Investigation: B.Z., I.S.C., R.S.B., W.C.D., T.S., and G.A.d.W. Visualization: B.Z. and T.S. Funding acquisition: I.S.C., R.S.B., and B.Z. Project administration: I.S.C. and R.S.B. Supervision: I.S.C. and R.S.B. Writing–original draft: B.Z. Writing–review and editing: I.S.C., R.S.B., J.M.S., E.K.T., W.C.D., T.S., and G.A.d.W. **Competing interests:** The authors declare that they have no competing interests. **Data and materials availability:** All data needed to evaluate the conclusions in the paper are present in the paper and/or the Supplementary Materials. All data are available at the NOAA National Centers for Environmental Information: https://www.ncei.noaa.gov/access/paleo-search/study/35473.

Submitted 16 September 2021
Accepted 4 February 2022
Published 23 March 2022
10.1126/sciadv.abm4346